The final publication is available at

https://doi.org/10.1002/elan.201900515

Discrimination and provenances of Phoenician Red Slip Ware using both the solid state electrochemistry and petrographic analyses

Lucilla Fabrizi[a], Lorenzo Nigro[b], Federico Cappella[b], Federica Spagnoli[b], Michele Guirguis[c], Ana Maria Niveau de Villedary y Mariñas[d], María Teresa Doménech-Carbó[e], Caterina De Vito*[a], Antonio Doménech-Carbó*[f]

[a] Department of Earth Sciences, Sapienza University of Rome, P.le Aldo Moro 5, Rome, Italy.
[b] ISO - Italian Institute of Oriental Studies, Sapienza University of Rome, P.le Aldo Moro 5, Rome, Italy
[c] Department of History, Humanities and Educational Sciences, University of Sassari, Piazza Università 21, Sassari, Italy
[d] Department of History, Geography and Philosophy, University of Cádiz Cadiz, C/ Paseo Carlos III, nº 9, 11003, Cádiz, Spain
[e] Institut de Restauració del Patrimoni, Universitat Politècnica de València, Camí de Vera 14, 46022, València, Spain.
[f] Departament de Química Analítica. Universitat de València. Dr. Moliner, 50, 46100, Burjassot (València), Spain.

* Corresponding authors; e-mail: caterina.devito@uniroma1.it; antonio.domenech@uv.es.

Abstract

Solid state electrochemistry based on the voltammetry of immobilized microparticles (VIMP) methodology is applied to a series of 80 Phoenician Red Slip samples from the archaeological sites of Motya (Sicily, Italy), Mogador (Morocco), Ramat-Rahel (Israel), Sulky (Sardinia, Italy), Tas Silg (Malta), Pantelleria (Italy), and Cádiz (Spain), dated from the 8th to the 6th century BC. Upon attachment of sub-microsamples to graphite electrodes in contact with aqueous H_2SO_4 electrolyte, voltammetric features due to the reduction of Fe(III) minerals and the oxidation of Fe(II) ones, complemented with electrocatalytic effects on oxygen reduction and oxygen evolution reactions, provide characteristic electrochemical fingerprints for pottery samples. A consistent sample grouping discriminating between different vessels of pottery among that recovered in the same site, and between equivalent potteries from different sites, is obtained, all results being consistent with morphological, compositional and mineralogical data. Petrographic analysis supports the grouping, defining the manufacture and firing procedure for the different archaeological context.

Keywords: Electrochemistry; Petrography; Ceramics; Phoenician.

1. Introduction

At the beginning of Iron Age, Phoenician culture spread over the the Syro-Palestinian coast, coastal Anatolia and Cyprus. Phoenician culture is largely indebted to the Canaanite Late Bronze Age traditions but is enriched with Aegean and Mediterranean experiences brought by the Peoples of the Sea at the end of the second millennium BC [1,2]. The Phoenician expansion along the trade routes all over the Mediterranean since the 14th century BC, led to the establishment of new colonies at the beginnings of the 8th century BC [1,2]. *Red Slip Ware* is the typical Phoenician ceramic production, it is characterized by a shiny deep red coating on its surface, and, as affirmed by Patricia Bikai [3], "*it is the Red Slip repertoire that goes with colonists to the western sites*". This typological class of ceramic was produced in the Levant during the Iron Age, since the end of the 11th century BC and represents the most distinguishing luxury pottery among the Phoenicians from the 11th to the 6th century BC both in the Levant and in Western colonies, as it was used in communal banquets, as well as in religious and funerary celebrations [1-3].

The occurrence of a great quantity of sherds of *Red Slip Ware* in earliest archaeological layers of the western Phoenician settlements can testify to the early stages of the colonization of the Mediterranean area dating back to the 8th century BC. The *Red Slip Ware* is an important cultural marker that followed the Phoenician traders across the Mediterranean [1,2]. From this point of view, defining both the production technique and the raw materials involved in the *Red Slip Ware* production can provide information on the timing and the dynamics of the Phoenician expansion through the Mediterranean Sea.

In the panorama just outlined, reconstructing the production methods of the *Red Slip Ware*, common to geographically distant contexts and strongly representative of Phoenician culture, will allow to outline the evolution and changes in the technique used, and understand if, and how, has been modified in the different geographical areas. The study will be useful to reconstruct the circulation dynamics of these artifacts and to increase the knowledge of Phoenician production techniques, contributing to the historical-cultural study of the population.

The elucidation of the chemical and mineralogical composition of archaeological ceramic materials are essential to achieve information on their provenance and technology [4], as illustrated by recent studies, among others, on Athenian Black-Gloss ceramic slips [5], luster pottery [6], and Terra Sigillata [7]. Pottery can be considered of particular interest by their relative abundance compared

to other finds types in archaeological sites. Its manufacturing is influenced by several factors, namely, temperature, duration, and reducing/oxidizing conditions of firing [8-10], defining a technological fingerprint for each production [11-15].

Pottery characterization is made from optical and electron microscopies, elemental analysis, thermal analysis, X-ray diffraction, infrared and Raman spectroscopies, among other techniques, yielding the essential information on the provenance and technology of the archaeological samples [11-16]. One frequent problem in field archaeology is the discrimination between different types of pottery when it is recovered from the site in fragmented state and/or when there is no well-defined stratigraphy and/or when productions from different provenances are accumulated in the same site. In these cases, the use of several of the above methods is conditioned by their difficulty to be applied to a high number of samples and/or the requirement of relatively large amounts of sample.

In this context, solid state electrochemistry can be used as a technique complementing the available analytical methodologies. Here, we report an approach based on the voltammetry of microparticles (VIMP). This methodology, developed by Scholz et al. [17,18], consist of the record of the voltammetric response of a solid sample abrasively attached to an inert electrode (graphite usually) when it is put into contact with a suitable electrolyte. Due to its inherently high sensitivity an essentially non-invasive sampling the VIMP has been applied for studying different types of cultural heritage [19]. In particular, this technique was previously used for characterizing different iron, lead and manganese species in ceramic materials [20-23], composition of raw materials [24], characterization of and discriminating the production centers of archaeological glasses [25-27] and Roman [28] and Inka [29] pottery.

In the current work, the VIMP technique has been expanded to face the archaeological problem of the possible correlation between pottery production from different centers. Voltammetric data have been applied to a set of 80 *Red Slip Ware* samples unearthed in archeological contexts of different countries of the Mediterranean World (Figure 1) *i.e* Israel, Malta, Italy, Spain, Morocco, dating back from the early 8th century to the beginning of the 6th century, in order to discriminate different productions. Voltammetric data were performed at sample-modified graphite electrodes in contact with air-saturated aqueous acidic media (0.10 M H_2SO_4). It is pertinent to note that the sampling process requires sample amounts at the micro-nanogram level, easily extracted with a microscalpel from the ceramic body to be abrasively transferred to graphite pencil electrodes [30]. To ensure representativity, for each object at least three samples from different spots of the ceramic body were

taken. The comparison of the electrochemical results with petrographic analysis permits an effective grouping of the samples, discriminating sherds from different provenances as well as productions with different age of the same site.

1.2. Archaeological context and sampling

Phoenician colonization is a complex phenomenon that developed in a very broad time span, between the 14th and the 8th century BC, involving a wide area from Cyprus to the Western Mediterranean, including the Iberian Peninsula and the Atlantic coasts of Morocco [1,2]. For its large scale and long duration, the study of the ceramic repertoire from the Phoenician cities of this area, as Lebanon, Israel/Palestine, Morocco, Malta, Italy (Sicily, Sardinia), and Spain is useful to reconstruct the technological level and the development of the pottery technology both in the motherland and in the colonies, since the early stages of the Phoenician colonization [1,3].

In this study, 80 *Red Slip Ware* pottery fragments of different shapes of vessels dating back from the early 8th century to the beginning of the 6th century BC are studied. The most abundant ceramic repertoire was unearthed at Motya (Sicily, Italy), the samples being dated from the 8th to 6th century BC [31,32]. A second repertoire of *Red Slip Ware* fragments come from Sulky (Sant'Antioco, Sardinia, Italy). This city was founded by the Phoenicians around 800-770 BC and represents the oldest Phoenician settlement on that island [33,34]. A third group of samples come from the modern city of Cádiz (Andalusia, Spain), which is the ancient Phoenician city of Gadir [35]. The earliest occupation by Phoenicians was dated back around 820-800 BC. Samples come from "Cánovas del Castillo" site located at the center of the modern city, occupied since the 8th century BC. Other samples come from the 6th century BC tombs of the ancient Necropolis [35]. Finally, samples of various collections (Museum of the Near East, Egypt and Mediterranean, Sapienza University of Rome, Italy) from Ramat-Rahel (Israel), Mogador (Morocco), Pantelleria (Italy) and Tas Silg (Malta) provide a series of useful comparisons. Samples analyzed in this study have been selected from well known and already published archaeological contexts, with reliable stratigraphy and absolute dating. The description of such samples is summarized in Table 1. Figure 1 shows the most representative samples of each contest (more detailed data are given in the Supplementary Information, Table S.1).

2. Experimental
2.1. Instrumentation and methods

VIMP measurements were performed at 298 K in a three-electrode cell using a CH I660C device (Cambria Scientific, Llwynhendy, Llanelli UK). Air-saturated aqueous 0.10 M H_2SO_4 solution (Panreac) was used as a supporting electrolyte; no deaeration was performed in order to mimic operating conditions for in-field analysis using available portable equipment. Graphite bars of 2 mm diameter (Alpino, BH type) were used, after incorporation of pottery samples, as a working electrodes, the three-electrode arrangement being completed by a platinum wire auxiliary electrode and an Ag/AgCl (3 M NaCl) reference electrode. The analysis of ceramic bodies was carried out by extracting, with the help of a scalpel, 2–5 μg of sample from the section of the ceramic fragment and powdering it with an agate mortar and pestle. The material was extended and grouped forming a fine coating on the plane face of the mortar and then was abrasively transferred onto the graphite electrode as customary in VIMP experiments [17-19].

Petrographic analysis in thin section was performed to define microstructure and porosity system of the sherds, using a Zeiss D-7082 Oberkochen polarized optical microscope (Earth Sciences Department of Sapienza, University of Rome). According to Whitbread criteria for ceramic materials, inclusions, matrix and porosity of both the *Red Slip* and body have been examined for samples of each archaeological context.

3. Results and Discussion
3.1. Petrographic analysis
The essential characteristics of the structure of each sherd, *i.e.* the nature of the inclusions (packing and size distribution) and groundmass, the features of porosity system, have been investigated, identifying the main features of samples with different provenance [36-38]. Figure 2 shows micro photos of representative thin sections of each context.

Petrographic analysis of Motya samples showed moderately sorted inclusions, from sub-angular to rounded inclusions. The size of the inclusions has a unimodal distribution and varies in the range of 2.5 – 0.05 mm. The mineralogical composition is made of fragments of quartz as the predominant component, often associated with fragments of carbonate sedimentary rocks, microfossils, fragments of feldspars (plagioclase and K-feldspar) and nodules of iron compounds. Rare clay pellets and grog inclusions occur along with mica crystals and microfossils. The optical active matrices of the samples are calcareous or sub-calcareous with a homogeneous reddish-light brown color (in plane parallel light) and a reddish-brown color (in crossed polarize light). The porosity system (5-20%) is represented by a prevalence of vughs and elongated voids (< 2.0 mm), with a

minor number of vesicles (< 0.5 mm). However, few samples show different petrographic features that allow hypnotizing the provenance from other workshops and a probably imported origin. In particular, MC.09.2466/01 and MC.10.2954/3 samples present pores due to carbonized organic material remains and a higher occurrence of clay pellets. Moreover, clinopyroxene fragments are the main inclusions of MC.07.1685/71 sample and grog fragments are dominant in MC.10.2943/1.

The samples from Sulky, Sardinia, contain poorly sorted inclusions (1.2 – 0.1 mm) with a unimodal distribution, the roundness varies from angular to rounded. These samples are characterized by the dominant presence of quartz fragments, common inclusions of igneous rock, plagioclase and K-feldspar and minor amounts of sandstone and nodules of Ti-Fe oxides. Fragments of carbonate sedimentary rocks are very rare or totally absent. The non-calcareous optical active matrix includes abundant micro-crystalline phases and presents a non-homogeneous color (light brown color in plane parallel light and a reddish brown/ochre color in crossed polarize light, with dark red or dark brown areas). Porosity system (3-10%) shows the occurrence of vughs (< 2.0 mm) and elongate voids with parallel alignment to the margin of the sample; the presence of vughs >2.0 mm is sporadic.

The samples from Cádiz show sub angular or sub-rounded inclusions (0.7 – 0.05 mm), moderately sorted. Bimodal or unimodal distributions of the size inclusions are present. Quartz crystals fragments are predominant and often associated with common fragments of carbonate sedimentary rocks and microfossils. Minor amounts of fragments of feldspars crystals, Fe nodules, and fragments of calcite are present, whereas fragments of mica and siliceous sedimentary rocks occur rarely. The matrix is always optically active, with a homogeneous beige-light brown color in plane polarized light and ochre-brown in crossed polarizer light. The porosity system (3-10%) is composed by vughs (≤0.5 mm) along with minor vesicles (≤0.5 mm). The porosity is generally aligned with the walls of the vessels.

The four samples from Ramat-Rahel show inclusion with shapes from sub-rounded to rounded, moderately or well sorted inclusions (1.2 -0.05 mm). The size of the inclusions has a unimodal distribution. Fragments of carbonate sedimentary rocks, often with microfossils, are dominant and associated with frequent quartz fragments and few Fe nodules. Very few or rare are the fragments of feldspar, pyroxene, biotite and clay pellets. Porosity (5-10%) is around mainly made of vughs (< 2.0 mm) and micro-vesicles, aligned with the walls of the vessels. The moderate optical activity of

the calcareous matrix presents a homogeneous color (brown in plane polarized light and reddish brown in crossed polarized).

Petrographic analysis of the samples from Mogador reveals the presence of sub-angular or sub-rounded, inclusions (0.3 – 0.05 mm), moderately sorted and unimodal size distribution. The mineralogical composition is dominated by fragments of quartz, with common microfossil and minor amounts of mica, Fe nodules, carbonate sedimentary rock and fragments of calcite. Feldspar is very few, and sandstone fragments are rare. The homogeneous optically active matrix shows beige/light-brown color in plane polarized light and ochre–brown color in crossed polarized. The porosity varies from 3% to 5% of the total of the volume, consisting mainly of vesicles (≤0.5 mm), with few vughs (≤0.5 mm), sub-aligned with the vessels wall.
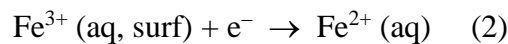
The two Maltese samples from Tas Silg present inclusions with shapes from sub-angular to rounded, (1.2 – 0.01mm). The inclusions are poorly or moderately sorted, with unimodal size distributions. Fragments of carbonate sedimentary rocks containing microfossils are dominant, in association with abundant fragments of carbonate sedimentary rocks, quartz fragments, and microfossils. Inclusions of feldspar and Fe nodules are few, whereas the inclusions of sandstone are rare. In sample M3365 inclusions of mica and argillaceous inclusion also occur. The optical active calcareous matrix is almost homogeneous in color, brown-ochre in plane polarized light and reddish brown in crossed polarized. The porosity systems (10%) shows vughs (< 2.0 mm) with few micro-vesicles, aligned with the vessels walls.

Finally, the only sample from Pantelleria (Italy) has inclusions from sub-angular to sub-rounded, moderately sorted (0.03-0.05 mm) and the grain size distribution is unimodal. The analysis identifies frequent fragments of quartz, of carbonate sedimentary rock with microfossils, and clay pellets; common Fe nodules and microfossils; few fragments of feldspar, mica and sandstone and rare fragments of calcite. The calcareous matrix is not homogeneous with darker brown stripes in the middle, it is ochre colored in plane polarized light, and reddish-brown colored in crossed polarized. The percentage of porosity is around 3-5% with vughs (<2 mm) and microvesicles, sub-aligned with the vessel wall. A summary of the petrographic features is provided as Supplementary information (Table S.1).

3.2. Voltammetric pattern

The voltammetric response of microparticulate deposits of pottery samples on graphite electrodes was recorded in contact with air-saturated 0.10 M H_2SO_4 aqueous solution. Figure 3 illustrates the square wave voltammograms of a,b) sample MD.07.2219/56 (two replicate measurements) and c,d) hematite, sample MC.11.2491/51 and two replicate measurements on a 50 %wt mixture of hematite and that sample. In the initial negative-going potential scan (Figure 3 a, c), cathodic peaks at ca. +0.60 (C1), +0.20 (C2) −0.15 (C3) and −0.65 (C4) appear, being limited by large currents at ca. +1.0 V and −1.0 V which correspond, respectively to the oxygen evolution reaction (OER) and the hydrogen evolution reaction (HER). In the positive-going potential scan voltammograms (Figure 3 b, d), anodic signals around +0.4 (A1) and +0.6 V (A2) appear preceding a more intense wave at +0.85 V (A3).

As judged upon comparison with the voltammogram of hematite in Figure 3c and literature data on HCl electrolytes [22-24,28,29,39,40], the signals C1-C4 correspond to the reduction of hematite and other Fe(III) mineral following different pathways. It is pertinent to note that the reduction of Fe(III) species is sensitive to the chemical composition but also to the crystallinity and degree of hydration of the electroactive components [28,29] so that the prominent signal C1 can be attributed to the reduction preceded by proton-assisted surface dissolution (roughly, CE mechanism) forming surface, solution-like Fe(III) species reduced to Fe(II) in solution phase. For hematite, this can be represented as:

$$Fe_2O_3 \text{ (solid)} + 3x\text{H}^+ \text{ (aq)} \rightarrow (Fe_{2-x}O_{3-3x/2})\{x\text{Fe}^{3+}\} \text{ (aq, surf)} \quad (1)$$

$$Fe^{3+} \text{ (aq, surf)} + e^- \rightarrow Fe^{2+} \text{ (aq)} \quad (2)$$

whereas the signals C2-C4 can be assigned to 'direct' reductive dissolution processes:

$$Fe_2O_3 \text{ (solid)} + 6\text{H}^+ \text{ (aq)} + 2e^- \rightarrow 2Fe^{2+} \text{ (aq)} + 3H_2O \quad (3)$$
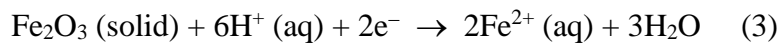
in which the appearance of different signals reflects the differences in chemical composition, shape and size of mineral grains and the degree of hydration and crystallinity of the minerals, the peak C4 corresponding to the 'direct' reduction of crystalline hematite superimposed to that of dissolved oxygen (oxygen reduction reaction, ORR) [39,40].

The signals A1, A2 can be attributed to the anodic counterparts of the reduction of Fe(III) minerals (square wave voltammograms display simultaneously cathodic and anodic processes) and/or the oxidation of Fe(II) minerals (such as falayite, gehlenite, etc.) [22,23]. As judged by blank

experiments using different iron minerals, the anodic signal A3 can be mainly assigned to the oxygen evolution catalyzed by crystalline hematite.

The relevant point to emphasize is that the relative height of the different voltammetric signals exhibits significant variations from one sample to another. This can be seen in Figure 4 where the negative-going square wave voltammograms of samples a) MD.07.2219/56, b) Mogador 8, c) MC.09.2466/01 and d) ML.07.44/4 are depicted. Here, semi-derivative convolution of current/potential curves has been performed in order to increase peak resolution.

For grouping purposes, it is pertinent to note that: i) since the net amount of sample transferred onto the graphite electrode cannot be accurately controlled (a common characteristic of the VIMP), the absolute values of the peak currents for each sample vary in replicate experiments, and ii) given the abrasive nature of the electrode conditioning, there is a different background current at each potential in the aforementioned replicate experiments.

3.3. VIMP grouping

The peculiar characteristics of VIMP data imply that, for grouping purposes, different pairs of currents (and or their ratios) rather than the isolated currents have to be used. For this purpose, the peak currents were measured using the base line depicted in Figure 4a.

First of all, the self-consistency of electrochemical data was tested combining the data for all archaeological samples. Figure 5 shows the representation of $I(A2)$ vs. $I(A1)$ (all replicate experiments appear as individual data points) which clearly defines a linear tendency suggesting that both electrochemical processes are directly related and due to a pair of species common to all samples. In contrast, the plots combining other pairs of signals clearly diverge from the above, thus denoting that the corresponding voltammetric signals have to be attributed to non-related electroactive species. This can be seen in Figure 6, where plots of $I(A2)$ vs. $I(A3)$ for a) Motya, b) Mogador and Sulky, c) Ramat-Rahel and Tas Silg, d) Cádiz (Necropolis and Cánovas street site) are depicted. One can see that data points for the different provenances appear to fall in different areas of the diagram.

In order to interpret the possible voltammetric grouping of pottery samples it is pertinent to consider the solid-state character of the involved electrochemistry. Figure 7 depicts a scheme of a microparticulate deposit of ceramic material consisting of a distribution of solid particles onto the surface of the graphite electrode. As a result, a certain area of the electrode, S, is covered by ceramic particles so that the graphite surface exposed to the electrode is S_o-S, S_o being the total area

of the graphite bar potentially in contact with the electrolyte. Let us consider two separate voltammetric signals corresponding to redox processes displayed by two different components A and B of the ceramic body. To describe the observed relationships between the peak currents $I(A)$, $I(B)$, for these signals one can use the theoretical models on the topotactic oxidation/reduction of ion-insertion solids [41-45] or the oxidative/reductive dissolution of electroactive solids [46,47]. In our case, there is a peculiar, intermediate, situation in which the electroactive Fe(III) and Fe(II) compounds are in the form of microcrystals embedded into a non-electroactive crystalline matrix of silicates and aluminosilicates, as schematized in Figure 7. Then, it is conceivable that their electrochemistry proceeds similarly to that of ion-insertion solids, the redox reaction starting at the crystal/base electrode/electrolyte three-phase junction, further expanding to the whole crystal. In these circumstances, the currents become proportional to the perimeter of the three-phase boundary [41-45].

Since in general there is a certain background contribution to the signals A and B, the peak currents for the processes A and B in a voltammogram recorded when a certain amount of sample, covering a surface S, has been attached to the graphite electrode, will be:

$$I(A) = \varepsilon_{backA}(S_o\text{-}S) + \varepsilon_A f_A p \quad ; \quad I(B) = \varepsilon_{backB}(S_o\text{-}S) + \varepsilon_{AB} f_B p \quad (4)$$

where ε_A, ε_B, ε_{backA}, ε_{backB} represent the respective coefficients of electrochemical response for the processes displayed by the components A and B and the bare graphite at the potentials at which the processes A and B occur, respectively. In the above expressions p denotes the perimeter of the particle of ceramic material, and f_A, f_B, the fraction of the components A and B exposed to the before mentioned three-phase junction. The perimeter p can be taken as proportional to the area S introducing a proportionality coefficient g. This coefficient will depend on the geometrical characteristics of the crystals (for instance, for cuboid crystals of size a, the perimeter will be $p = 4S^{1/2}$), so that $p = gS^{1/2}$. Then, one can write:

$$I(A) = \varepsilon_{backA}(S_o\text{-}S) + \varepsilon_A f_A g_A S^{1/2} \quad ; \quad I(B) = \varepsilon_{backB}(S_o\text{-}S) + \varepsilon_B f_B g_B S^{1/2} \quad (5)$$

In different voltammetric experiments, different amounts of sample, and hence, different electrode coverages will be produced. Then, eliminating S between Eqs. (4) and (5) one obtains a relatively complicated polynomial relationship between $I(B)$ and $I(A)$ which applies regardless the amount of

sample deposited onto the electrode, consistent with experimental data in Figures 8 and 9 (*vide infra*). In the case of low electrode coverage ($S \ll S_o$) the relationship tends to:

$$I(B) = (\varepsilon_B g_B f_B / \varepsilon_A g_A f_A)I(A) + S_o(\varepsilon_{backA} g_A f_A - \varepsilon_{backB} g_B f_B) \qquad (6)$$

While in the case of complete coverage ($S \approx S_o$),

$$I(B) = (\varepsilon_A g_A f_A / \varepsilon_B g_B f_B)I(A) \qquad (7)$$

In both limiting cases predicting a linear relationship between $I(B)$ and $I(A)$.

Figure 8 compares the plots of $I(C3)$ vs. $I(C1)$ for: a) Motya; b) Ramat-Rahel; c) Tas Silg and Pantelleria samples; d) Motya samples MC.09.2466/01, MC.07.1685/71, MC.10.2954/3 and MC.10.2943/1 whose petrographic analysis suggests being products of importation. In spite of some dispersion, the experimental data from Motya can be fitted to potential function (continuous lines in Figure 8). Interestingly, the samples from Ramat-Rahel and Tas Silg fall within the same tendency curve defined by Motya. Interestingly, data points for the samples from this site but attributed to importation are separated (although slightly) from the Motya curve. This separation is larger for the unique Pantelleria sample.

The samples from Sulky, Mogador and Cádiz define clearly different tendency curves. This can be seen in Figure 9 in which the $I(C3)$ vs. $I(C1)$ plots for a) Cádiz and b) Mogador and Sulky samples with their corresponding curves resulting from data fitting to potential laws (continuous lines), and the tendency curve obtained for Motya samples (dotted lines). Two features can be underlined: i) the samples from the two provenances define clearly separated tendency graphs, and, ii) the Cádiz samples from the from "Cánovas del Castillo" site (8th century BC are grouped in a different region to that of samples from Necorpolis (6th century BC). This second feature suggests that there is possibility of electrochemical discrimination of samples produced in the same center in different periods even when a quite similar manufacturing was carried out.

3.4. Discussion

The voltammetric grouping of *Red Slip* Phoenician pottery described in section 3.3 is supported by the petrographic analyses. The grouping of the samples based on the electrochemical data can

simultaneously reflect a different composition of the natural clay and a different condition of the firing environment (fugacity of the oxygen and control of the temperature). Indeed, the Fe content is variable in the composition of different deposits of clay [48], and its oxidation state and crystallinity degree may vary according to the condition of firing environment to which the raw materials with different composition have undergone [49,50]. In the studied samples, the not vitrified and optical active matrix suggest temperature not exceeding the 900°C [13,51]. Concerning Motya samples, the moderately sorted and fine grained inclusions suggest a careful selection of the raw material that probably have been sieved while the temperature and the condition of firing seem to be similar for all the samples. In fact, the homogeneous red color of the matrix testifies a controlled oxidizing atmosphere of firing, that permit the formation of hematite [13,51,52].

Petrographic analysis confirms the differences, highlighted by VIMP analyses, between Motya samples and Sulky samples (see Figure 9b), from different points of view. The starting raw materials results different, Sulky samples present a major content of igneous rock, plagioclase and K-feldspar and the matrix is non-calcareous. Moreover, the poorly sorted inclusions and the inhomogeneous color of the matrix suggest a rough preparation of the paste [37,38] and moderate level of technological background involved for the ceramic production under not well controlled firing conditions [53,54]. This environment can reduce the formation of hematite [52], and consequently generate an electrochemical signal different respect well oxidized samples.

The electrochemical analyses do not discriminate between samples from Motya and Ramat-Rahel (Figure 8 b), and indeed, these samples present many analogies also in the petrographic features. The well sorted inclusions suggest sieving procedure and a good selection of the raw material for the Israeli samples. The homogeneous reddish calcareous matrix suggests a very similar production technology for the two archaeological sites with controlled oxidized firing conditions [53,55].

Samples from Mogador made with well sorted fine grained inclusions, that have probably been sieved, present a good selection of raw material. The inclusions are carbonate rock fragments and microfossils mainly, resulting for these reasons, very different respect to samples of the other archaeological context, as clearly suggested by voltammetric data in Figures 6b and 9b. The homogeneous ochre color of the calcareous matrix allows to hypnotize that the control of firing conditions is fine and under oxidizing condition [52,56]. The ochre color of the matrix may be due to a higher content of Ca in the raw material, because this condition supports the formation of newly Ca-silicates phases and prevent an abundant hematite crystallization, leading to a ochre-beige color

of the matrix [50,52]. Consistently with these petrographic features, the voltammetric response of Mogador differs from the other red samples.

The well sorted and very fine-grained sand of quartz and microfossils of the samples from Cádiz suggest a good selection of sieved raw material. The calcareous matrix is homogeneous and ochre, suggesting controlled oxidizing atmosphere of firing and low amount of hematite [52,57,58]. However, significant petrographic differences were not highlighted between samples of the 6th century BC and 8th century BC from Cádiz, which seem to be made with a very similar raw clayey materials and similar technology of production.

Although the low number of accessible samples from Malta and Pantelleria does not permit the extraction of definite conclusions, some considerations can be added. Poorly-moderately sorted inclusions from Tas Silg samples suggest a modest procedure of selection of the raw materials. In this case the raw materials are rich in carbonate inclusions (fragments of carbonate sedimentary rocks fragments and microfossils) and the reddish color of the matrix suggests also a consistent content of hematite. The homogeneous color of the calcareous matrix infers a controlled atmosphere of firing [56-58]. While, the diffuse clay pellets present in the Pantelleria sample could be due to a not correct hydration of the paste during the modelling procedure [37,38]. Moreover, the aplastic inclusions are moderately sorted, these two elements lead to the conclusions that the modelling procedure was not very accurate [37,38]. This is the sample with the highest calcite content, both in terms of the nature of the inclusions and the micritic calcite contained in the matrix, consequently the raw materials used to produce this pot are very different from those used for the other samples. Finally, the calcareous and optically active matrix has an inhomogeneous and ochre-reddish brown color, suggesting not well controlled atmosphere of firing [59].

Conjointly considered, the above results clearly suggest that there is possibility of discriminating pottery productions from different provenances, thus opening the possibility of establishing a network of possible relations between different sites.

4. Conclusions

The solid state electrochemistry of archaeological pottery sub-microsamples attached to graphite electrodes in contact with aqueous 0.10 M H_2SO_4 electrolyte using the VIMP methodology consists

of well-defined responses associated to the reduction of Fe(III) minerals and the oxidation of Fe(II) ones. The voltammetric features recorded for pottery from the Phoenician sites of Motya (Sicily-Italy), Mogador (Morocco), Ramat-Rahel (Israel), Sulky (Sardinia-Italy), Tas Silg (Malta), Pantelleria (Italy), and Cádiz (Spain) permits to discriminate between: i) different manufacturing types from the same site; ii) pottery from different sites, and, iii) pottery production from the same site but made in different historical periods. The reconstruction of the manufacture procedure, based on the petrographic results, identify the technological level and the raw materials involved in each contest, and permit discrimination among the samples with different origin. Generally, the samples show a good selection of raw materials and the temperature of firing of the artifacts results below the 900 °C in controlled oxidizing atmosphere. Sardinia, Pantelleria represent the exceptions, with poorer manufacture technique, while Mogador and Cádiz samples presents less abundant amount of hematite, probably due to starting raw materials richer in Ca. These differences in raw materials and firing conditions can lead to the formation of Fe-based compounds with specific crystalline properties, which produce different electrochemical signals and allow the grouping of samples. Accordingly, the VIMP technique can be considered as a promising analytical tool complementing the scope of the available techniques usable for archaeometric purposes.

References

[1] P. Bartoloni, La ceramica fenica tra oriente e occidente. *Atti II Congr Internazionale Studi Fenici E Punici*; vol. II, pp. 641–53, **1991**.

[2] L. Nigro, *Vicino Oriente*, **2013,** XVII, 39–74.

[3] P.M. Bikai, The pottery of Tyre, Warminster, p. 75, **1978**.

[4] K.M. Towe, *J. Archaeol. Method Theory* **1999**, *6*, 1.

[5] M. Walton, K. Trentelman, I. Cianchetta, J. Maish, D. Saunders, B. Foran, A. Mehta, *J. Am. Ceram. Soc*. **2015**, *98*, 430.

[6] J. Pérez-Arantegui, J. Molera, A. Larrea, T. Pradell, M. Vendrell-Sanz, I. Borgia, B.G. Brunetti, F. Cariati, P. Fermo, M. Mellini, A. Sgamellotti, C. Viti, *J. Am. Ceram. Soc*. **2001**, *84*, 442.

[7] P. Sciau, S. relaix, C. Roucau, Y. Kihn, and D, Chabanne, *J. Am. Ceram. Soc*. **2006**, *89*, 1053.

[8] G.E. De Benedetto, R. Laviano, L. Sabbatini, P.G. Zambonin, *J. Cult. Herit*. **2002**, *3*, 177.

[9] M. Chatfield, *J. Archaeol. Sci*. **2010**, *37*, 727.

[10] M. Walton, K. Trentelman, M. Cummings, G. Poretti, J. Maish, D. Saunders, B. Foran, M. Brodie, A. Mehta, *J. Am. Ceram. Soc*. **2013**, *96*, 2031.

[11] E. Andaloro, C.M. Belfiore, A.M. De Francesco, J.K. Jacobsen, G.P. Mittica, *Appl. Clay Sci*. **2011**, *53*, 445.

[12] S. Kramar, J. Lux, A. Mladenovic, H. Pristacz, B. Mirtic, M. Sagadin, N. Rogan-Smuc, *Appl. Clay Sc*i. **2012**, *57*, 39.

[13] C. De Vito, L. Medeghini, S. Mignardi, D. Orlandi, L. Nigro, F. Spagnoli, P.P. Lottici, D. Bersani, *Appl. Clay Sci*. **2014**, *88–89*, 202.

[14] G.M. Mangueira, S. Teixeira, F.A. Silva, R.W.A. Franco, *Appl. Clay Sci*. **2016**, *129*, 88□91.

[15] C. De Vito, L. Medeghini, S. Garruto, F. Coletti, I. De Luca, S. Mignardi, *Ceram. Int*. **2018**, *44*, 5055.

[16] L. Medeghini, P.P. Lottici, C. De Vito, S. Mignardi, D. Bersani, *J. Raman Spectrosc*. **2014**, *45*, 1244.

[17] F. Scholz, B. Meyer, Voltammetry of solid microparticles immobilized on electrode surfaces, in *Electroanalytical Chemistry, A Series of Advances*. A.J. Bard, I. Rubinstein, I. Eds., Marcel Dekker, New York, vol. 20, pp 1–86, **1998**.

[18] F. Scholz, U. Schröder, R. Gulaboski, A. Doménech-Carbó, *Electrochemistry of Immobilized Particles and Droplets*, 2nd ed. Springer International Publishing, Berlin-Heidelberg, **2014**.

[19] A. Doménech-Carbó, M.T. Doménech-Carbó, V. Costa, *Electrochemical Methods in Archaeometry, Conservation and Restoration*, Monographs in Electrochemistry series, F. Scholz, Edit. Springer, Berlin-Heidelberg, **2009**.

[20] A. Doménech-Carbó, M.T. Doménech-Carbó, M. Moyá-Moreno, J.V. Gimeno-Adelantado, F. Bosch-Reig, *Electroanalysis* **2000**, *12*, 120.

[21] A. Doménech-Carbó, M.T. Doménech-Carbó, L. Osete-Cortina, *Electroanalysis* **2001**, *13*, pp. 927.

[22] A. Doménech-Carbó, S. Sánchez-Ramos, M.T. Doménech-Carbó, J.V. Gimeno-Adelantado, F. Bosch-Reig, D.J. Yusá-Marco, M.C. Saurí-Peris, *Electroanalysis* **2002**, *14*, 685.

[23] S. Sánchez-Ramos, F. Bosch-Reig, J.V. Gimeno-Adelantado, D.J. Yusá-Marco, A. Doménech-Carbó, *Anal. Bioanal. Chem.* **2002**, *373*. 893.

[24] G. Cepriá, J. Roque, J. Molera, J. Pérez-Arantegui, M. Vendrell, *Electroanalysis* **2007**, *19*, 1167.

[25] A. Doménech-Carbó, M.T. Doménech-Carbó, *Electroanalysis* **2005**, *17*, 1959.

[26] T. Palomar, M. García-Heras, M.A. Villegas, M.T. Sevilla, *Electroanalysis* **2011**, *23*, 521.

[27] A. Doménech-Carbó, M.A. Villegas, F. Agua, S. Martinez-Ramírez, M.T. Doménech-Carbó, B. Martinez, *J. Am. Ceram. Soc.* **2016**, *99*, 3915.

[28] F. Di Turo, N. Montoya, J. Piquero-Cilla, C. De Vito, F. Coletti, I. De Luca, A. Doménech-Carbó, *Appl. Clay Sci.* **2018**, *162*, 305.

[29] A. Doménech-Carbó, L. La-Torre-Riveros, W. Huanasoncco-Condori, D. Quispe-Guzmán, M.T. Doménech-Carbó, C.R. Cabrera-Martínez, M.C. Gutiérrez-Castillo, A. Pérez-Trujillo, J. Solid State Electrochem. In press, DOI: 10.1007/s10008-018-04182-5.

[30] D. Blue, W. Leyffer, R. Holze, *Electroanalysis* **1996**, *8*, 296.

[31] L. Nigro, Mozia nella preistoria e le rotte levantine: i prodromi della colonizzazione fenicia tra secondo e primo millennio a.C. nei recenti scavi della Sapienza, in A. Cazzella (a cura di): *Ubi Minor…. Le isole minori del Mediterraneo centrale dal Neolitico ai primi contatti coloniali*. Convegno di Studi in ricordo di Giorgio Buchner, a 100 anni dalla nascita (1914 – 2014) (Scienze dell'Antichità 22.2), Roma, pp. 339-362, **2016**.

[32] L. Nigro, F. Spagnoli, Landing on Motya. The earliest Phoenician settlement of the 8th century BC and the creation of a West Phoenician cultural identity in the excavations of Rome «La Sapienza» University - 2012-2016. Stratigraphy, architecture, and finds (Quaderni di Archeologia Fenicio-Punica/Colour Monograph 04). Rome: Missione archeologica a Mozia, **2017**.

[33] A. Unali, Sulky – Sant'Antioco, in M. Guirguis (a cura di): *La Sardegna fenicia e punica.* Sassari, pp.128-142, **2017**.

[34] M. Guirguis, *Riv Studi Fenici* **2005**, *XXXIII*, 1-2.

[35] A.M. Niveau-de-Villedary y Mariñas, *Vicino Oriente* **2018**, *XXII*, 91–109.

[36] A.M.W. Hunt, *The Oxford Handbook of Archaeological Ceramic Analysis*. Oxford University Press, Oxford, **2016**.

[37] P.S. Quinn, *Ceramic petrography. Interpret. Archaeol. Pottery Relat. Artefacts Thin Sect*. Oxford Archaeopress, Oxford, **2013**.

[38] C.L. Reedy, *Thin-section Petrography of Stone and Ceramic Cultural Materials*. Archetype, **2018**.

[39] A. Doménech-Carbó, M.T. Doménech-Carbó, H.G.M. Edwards, *Electroanalysis* **2007**, *19*, 1890.

[40] A. Doménech-Carbó, M. Lastras, F. Rodríguez, L. Osete-Cortina, *Microchem. J.* **2013**, *106*, 41.

[41] M. Lovric, F. Scholz, *J. Solid State Electrochem.* **1997**, *1*, 108.

[42] M. Lovric, M. Hermes, F. Scholz, *J. Solid State Electrochem.* **1998**, *2*, 401.

[43] K.B. Oldham, *J. Solid State Electrochem.* **1998**, *2*, 367.

[44] M. Lovric, F. Scholz, *J. Solid State Electrochem.* **1999**, *3*, 172.

[45] U. Schröder, K.B. Oldham, J.C. Myland, P.J. Mahon, F. Scholz, *J. Solid State Electrochem.* **2000**, *4*, 314.

[46] T. Grygar, *J. Electroanal. Chem.* **1996**, *405*, 117.

[47] T. Grygar, *J. Solid State Electrochem.* **1998**, *2*, 127.

[48] A. Meunier, *Clays*. Springer, Berlin-Heidelberg, 2005.

[49] L. Nodari, E. Marcuz, L. Maritan, C. Mazzoli, U. Russo, *J Eur Ceram Soc*. **2007**, *27*, 4665.

[50] J. Molera, T. Pradell, M. Vendrell-Saz, *Appl. Clay Sci.* **1998**, *13*, 187.

[51] Y. Maniatis, M.S. Tite, *J. Archaeol. Sci.* **1981**, *8*, 59.

[52] A. De Bonis, G. Cultrone, C. Grifa, A. Langella, A.P. Leone, M. Mercurio, *Ceram. Int.* **2017**, *43*, 8065.

[53] M. Maggetti, Technical aspects of the terra sigillata production: the pottery centre of Schwabegg (Augsburg, Germany, 2/3d c. AD). Editorial. pp. 221–228, **1995**.

[54] S. Gualtieri, B. Fabbri, *Ceram. Int.* **2016**, *42*, 17905.

[55] G. Eramo, M. Maggetti, *Anc. Ceram. – Anal. Compon.* **2013**, *82*, 16.

[56] C. De Vito, L. Medeghini, S. Mignardi, P. Ballirano, L. Peyronel, *J. Eur. Ceram. Soc.* **2015**, *35*, 3743.

[57] M.I. Carretero, M. Dondi, B. Fabbri, M. Raimondo, *Appl. Clay Sci.* **2002**, *20*, 301.

[58] B. Fabbri, S. Gualtieri, S. Shoval, *J. Eur. Ceram. Soc.* **2014**, *34*, 1899.

[59] L. Medeghini, L. Fabrizi, C. De Vito, S. Mignardi, L. Nigro, E. Gallo, C. Fiaccavento, *Ceram. Int.* **2016**, *42*, 5952.

Table 1. Characteristics of pottery samples in this study.

Site	Samples	Shape
Motya	MC.08.2435/05, MC.09.2466/01 MC.12.4427/4, MC.13.4441/27 ML.07.34/6, ML.07.44/4 ML.07.20/45, MD.16.1407/12,	Plate
	MC.13.4441/20, MC.11.1786/78 ML.07.34/5, MM.16.6047/149a	Chalice
	MC.08.2372b/1	Neck-ridge jug
	ML.07.20.123, MC.13.4446/11 ML.07.44/3b, MC.10.2954/3, MC.10.2943/1, MF.08.2641/3, ML.07.45/1	Carinated bowl
	MC.11.2491/32, MC.11.2491/29 MC.11.2462/63, MD.16.1406/1a-c	Bowl with everted rim
	MC.07.1685/71	Bowl
	MC.08.2372c/4a-d,	Open shape
	MF.09.2678/19	Skyphos
	MD.07.2219/84b, MD.07.2219/56 MC.11.2491/51, MC.11.2491/54	Closed shape
Cádiz	SS/10-12/UE 65.21, SS/10-12/UE 65.69 SS/10-14/ EF 35/UE 283.3, SS/10-12/UE 65.66 SS/10-12/UE 65.67, SS/10-14/ UE 147.2 SS/10-14/ UE 147.7, CC38/UE10.83 CC38/UE2b/2018.4, CC38/CRIBA/2018.5 CC38/C-4/2018.1, CC38/UE2c/2018.9.P1 CC38/UE2c/2018.9.P2, CC38/UE2c/2018.9.P3 CC38/UE2c/2018.9.P4, CC38/UE2c/2018.9.P5 CC38/UE2c/2018.9.P6, CC38/UE2c/2018.9.P7 CC38/UE2c/2018.9.P8, CC38/UE2c/2018.9.P9 CC38/UE2c/2018.9.P10	Plate
	SS/10-14/ EF 35/UE 283.1, SS/10-14/UE 65.42 CC38/C-4/2018.2	Bowl
	CC38/UE2b/2018.6	Bowl with handle
	CC38/UE2c/2018.10	Double-bowl
	CC38/UE2b.2018/1, CC38/UE2b/2018.7, CC38/UE2b/2018.8	Open shape
Sulky	CRON 3867.2 – S2	Plate
	CRON 3856 –S1, CRON 3867.4-S4 CRON 3846 – S6	Bowl with rim
	CRON 3846 – S5, CRON 3856 –S7 CRON 3867.1 - S8	Hemispherical bowl
	CRON 3873.6 – S3	Carinated bowl

Ramat - Rahel	M1028/1, M1230/1, M1739/2	Bowl with everted rim
	M83/997	Bowl with enlarged rim
Mogador	Mogador 8	Closed shape
	M3751 (Mogador 6), M3751 (Mogador 7) M3751 (Mogador 9)	Plate
Tas Silg	M3365	Shallow bowl
	M1239	Plate
Pantelleria	M3811	Plate

Figures

Figure 1. Archaeological sites from which the samples come. Tyre is indicated as a reference to the motherland and representative samples of each archaeological site involved in this investigation: MF.09.2678/19 from Motya, CRON 3867.4-S4 from Sulky, CC-38/UE10.83 from "Cánovas del Castillo" - Cádiz, SS 10-14/UE 65.42 from "Necropolis" - Cádiz, Mogador 8 from Mogador, M83/997 from Ramat-Rahel, M3365 from Tas Silg and M3811 from Pantelleria.

Figure 2. Thin-section micro-photographs representative of the production of different archaeological context in plane polarized light (PPL) and in cross polarized light (XP): Motya, sample MC.13.4441/27; Sulky, sample CRON 3856 –S7; Cádiz, sample CC38/UE2c/2018.9.P3; Ramat-Rahel, sample M1739/2; Mogador, sample Mogador 8; Tas Silg, sample M3365 and Pantelleria, sample M3811.

Figure 3. Square wave voltammograms of sample a,b) MD.07.2219/56 (two replicate measurements), c,d) hematite, sample MC.11.2491/51 and two replicate measurements on a 50 %wt mixture of hematite and that sample attached to graphite electrode in contact with air-saturated 0.1 M H_2SO_4. Potential scan initiated at a) +1.25 V in the negative direction; b) −0.85 V in the positive direction; potential step increment 4 mV; square wave amplitude 25 mv; frequency of 5 Hz. Two replicate experiments on freshly sample-modified electrodes are superimposed.

Figure 4. Square wave voltammograms, after semi-derivative convolution, of samples a) MD.07.2219/56, b) Mogador 8, c) MC.09.2466/01, and d) ML.07.44/4 attached to graphite electrodes in contact with air-saturated 0.1 M H_2SO_4. Potential scan initiated at a) +1.25 V in the negative direction; b) −0.85 V in the positive direction; potential step increment 4 mV; square wave amplitude 25 mv; frequency of 5 Hz.

Figure 5. Plots of *I*(A2) vs. *I*(A1) from square wave measurements such as in Fig. 3b for all samples in this study.

Figure 6. Plots of *I*(A2) vs. *I*(A3) from square wave measurements such as in Fig. 3b for: a) Motya, b) Mogador and Sulky, c) Ramat-Rahel and Tag-Silg, d) Cádiz (Necropolis and Cánovas del Castillo sites).

.

Figure 7. Scheme for the description of the electrochemistry of iron minerals (A, B) embedded into a non-electroactive matrix in pottery samples. Reduction of Fe(III) minerals involves coupled proton/electron entrance; catalytic effects on OER and other electrochemical processes are also possible.

Figure 8. Plots of I(C3) vs. I(C1) for pottery samples from: a) Motya; b) Ramat-Rahel; c) Tas Silg and Pantelleria; d) Motya samples MC.09.2466/01, MC.07.1685/71, MC.10.2954/3 and MC.10.2943/1, whose petrographic analysis suggests being products of importation. From square wave voltammograms after semi-derivative convolution such as in Figure 4. Experimental data superimposed in to the tendency curve (continuous lines) obtained by fitting the data points of Motya *plates* to a potential function; in d), this is accompanied by the curve for Mogador samples.

Figure 9. Plots of I(C3) vs. I(C1) for a) Cádiz and b) Mogador and Sulky samples with the corresponding tendency curves (continuous lines). The dotted line corresponds to the tendency curve obtained for Motya samples (Fig. 6a). From square wave voltammograms after semi-derivative convolution such as in Figure 4.

Figure 1.

MF.09.2678/19   CRON 3867.4-S4   CC-38/UE 10.83   SS 10-14/UE 65.42

MOGADOR 8   M 83/997   M 3365   M 3811

Figure 2

Motya

Sulky

Cádiz

Ramat-Rahel

Mogador

Tas Silg

Pantelleria
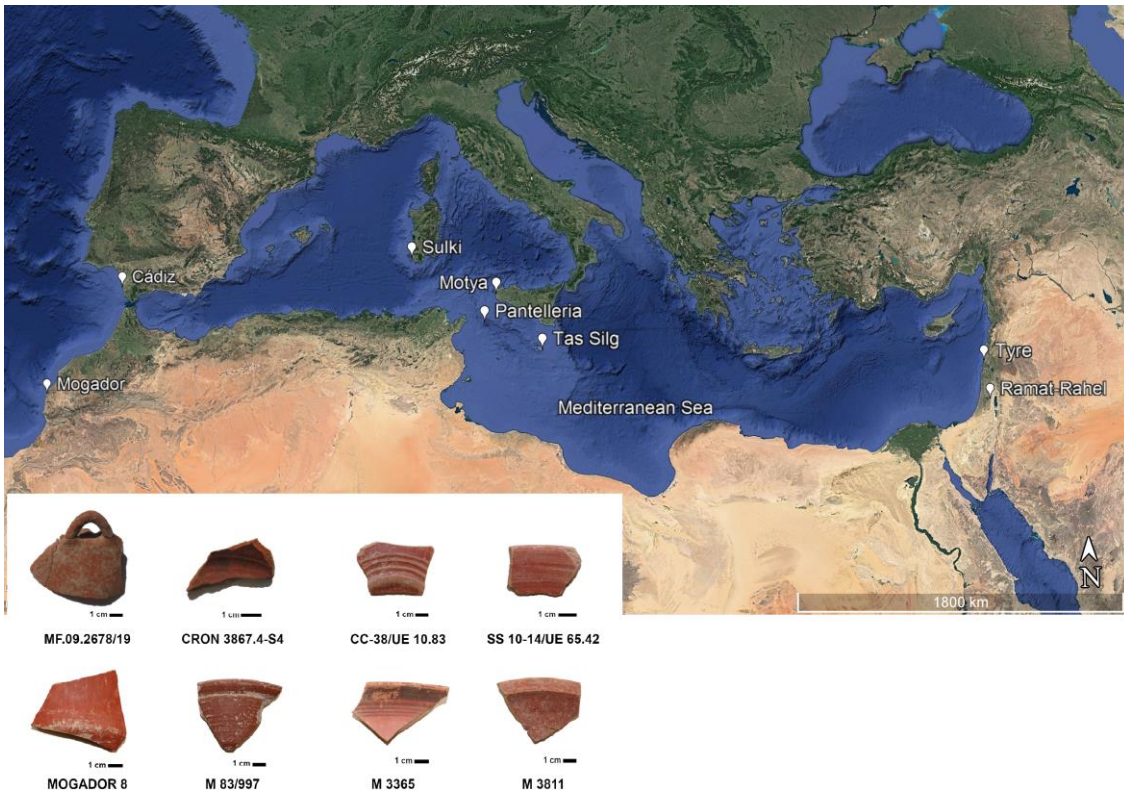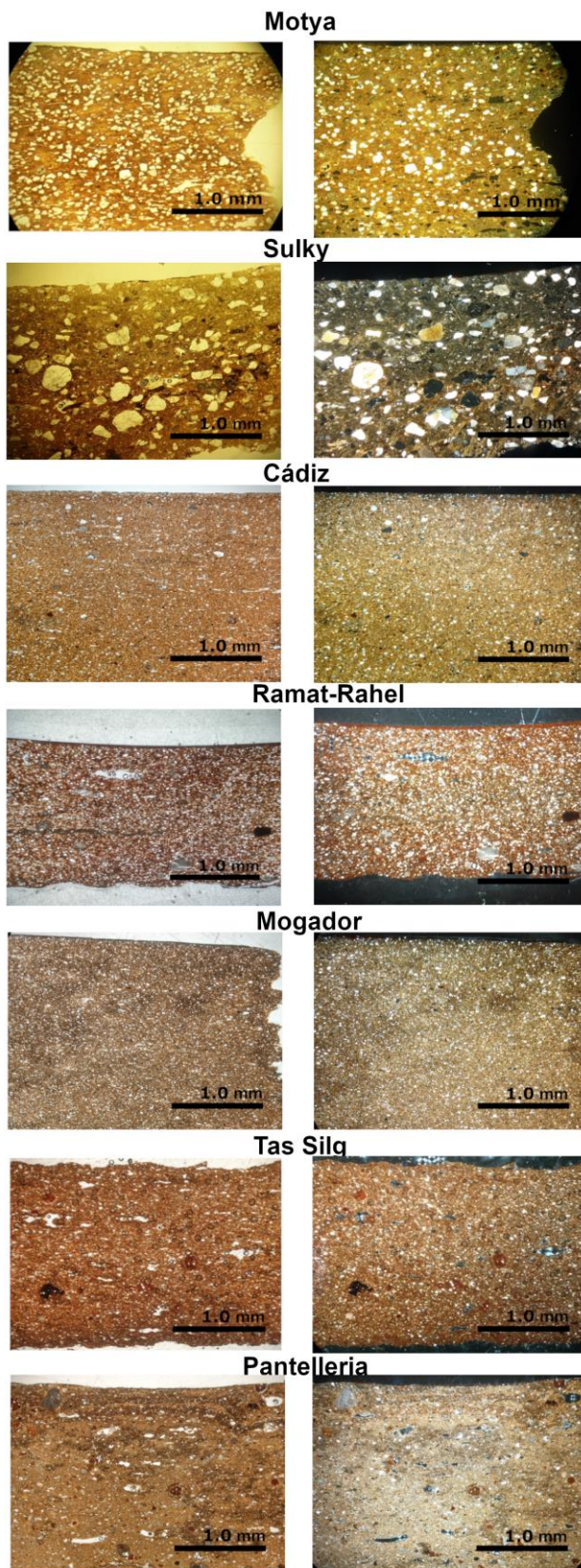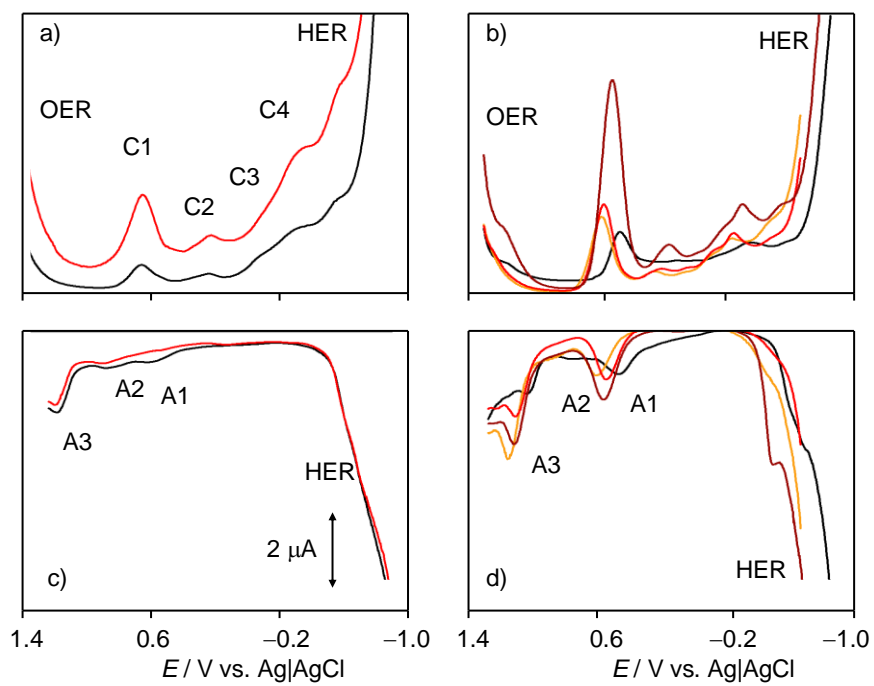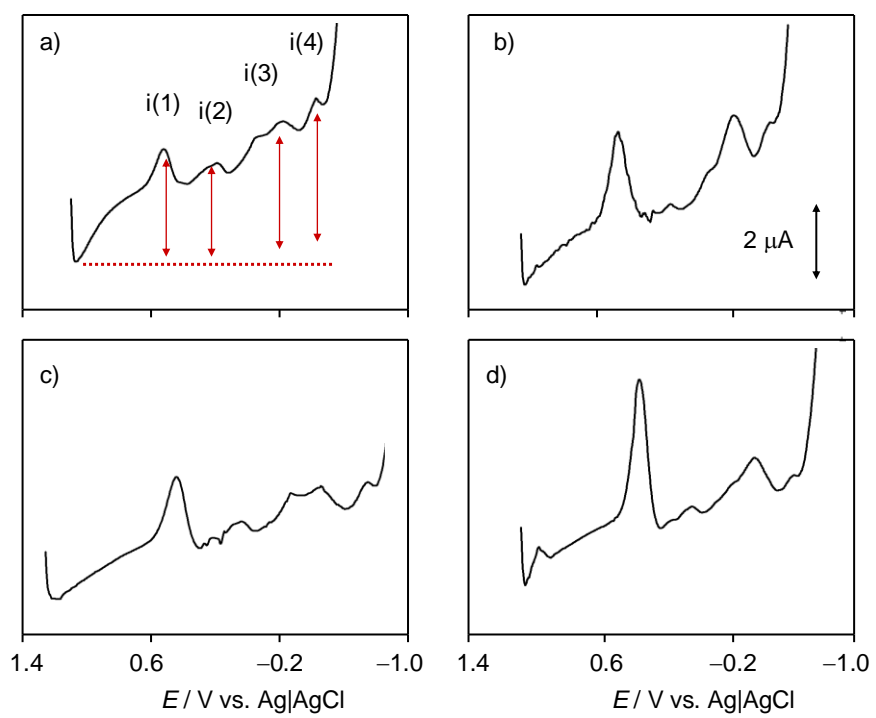
Figure 3.

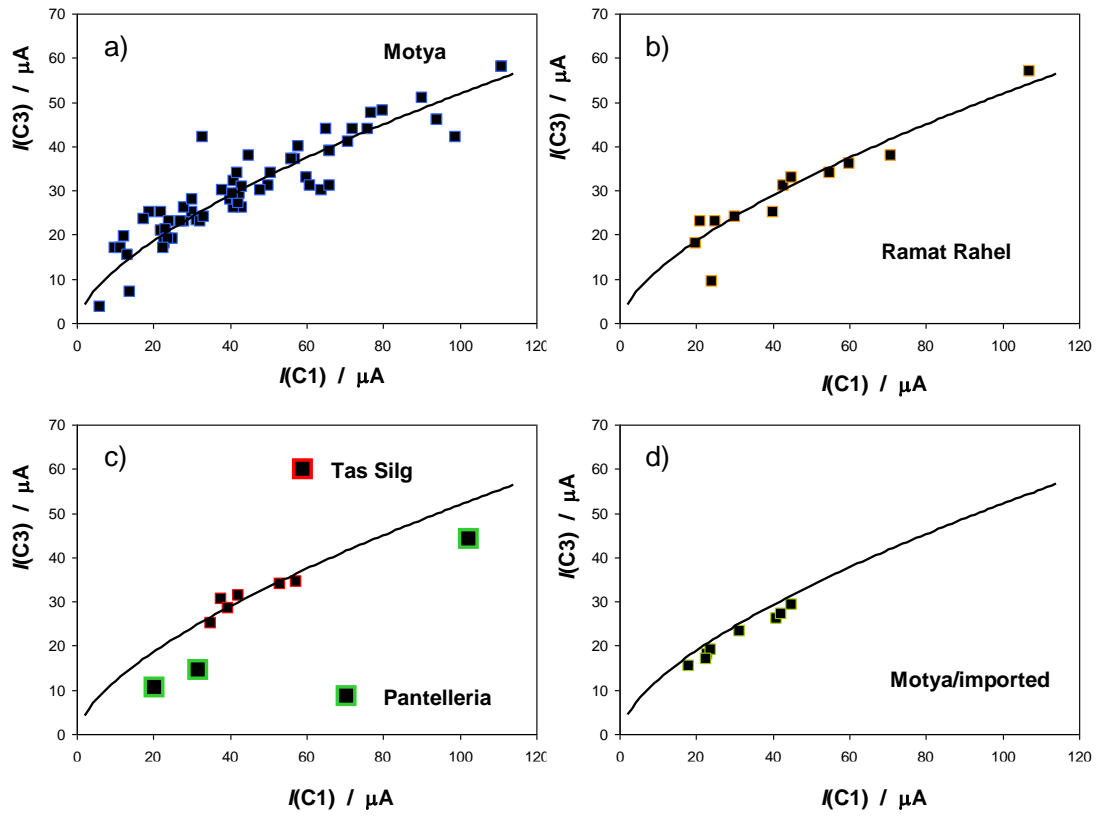**Figure 4.**

Figure 5.
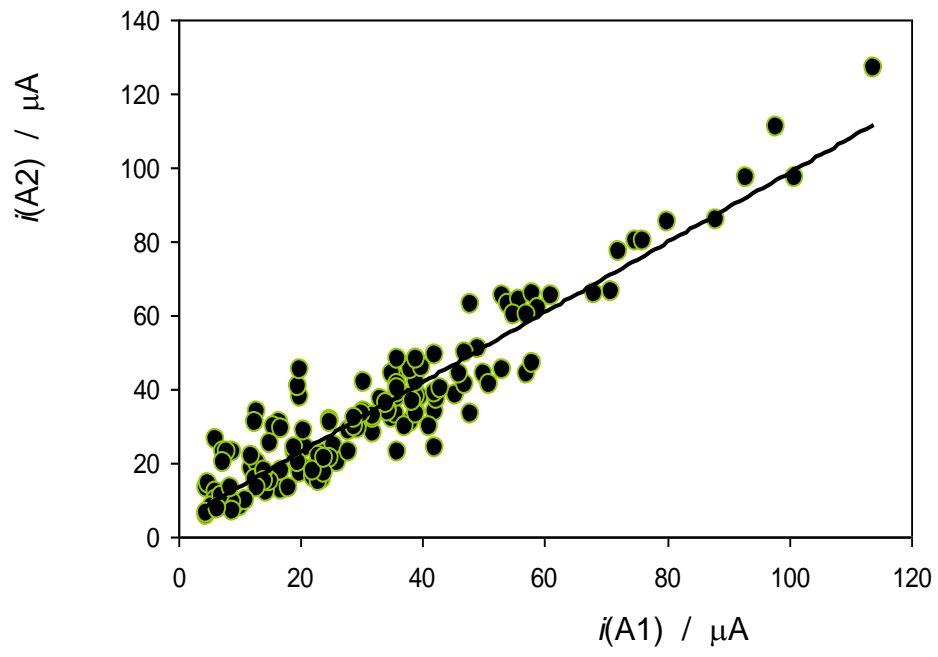
Figure 6.
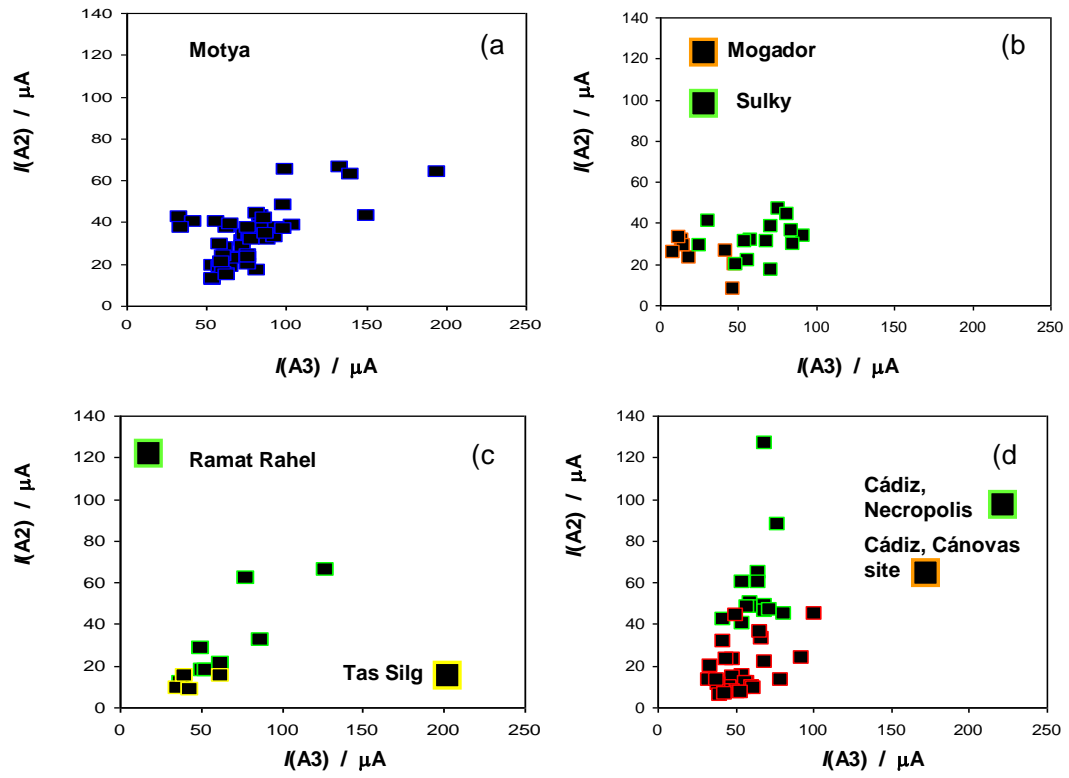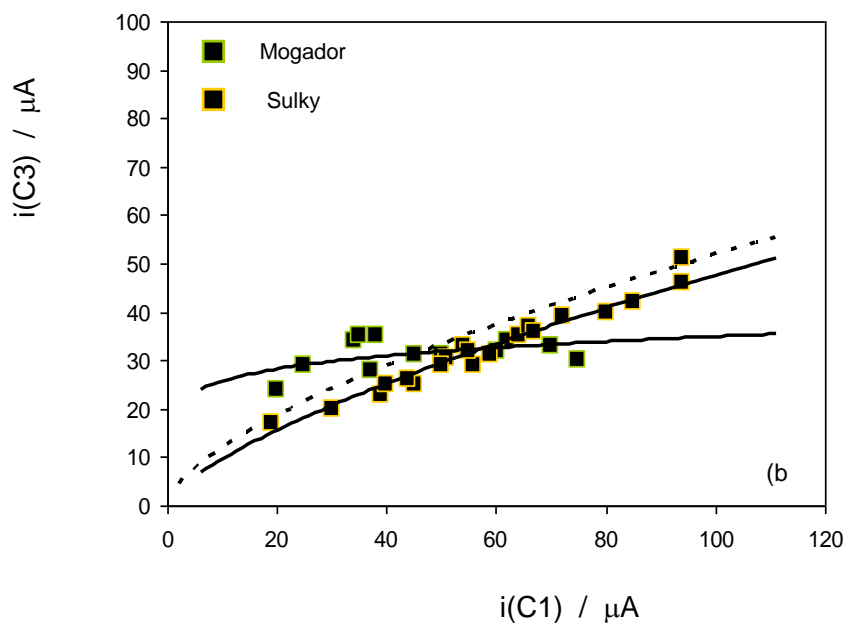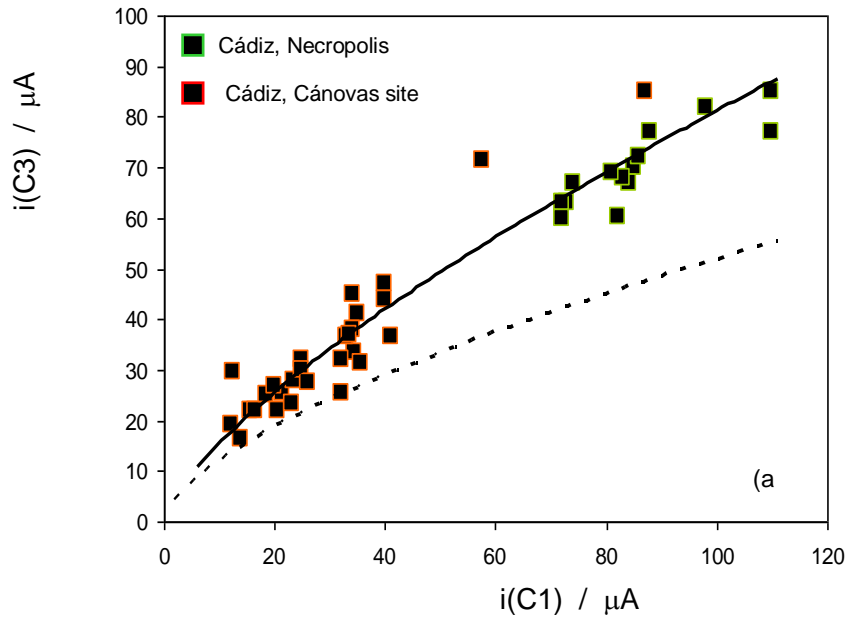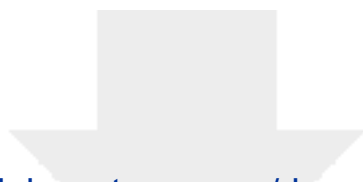
Figure 7.
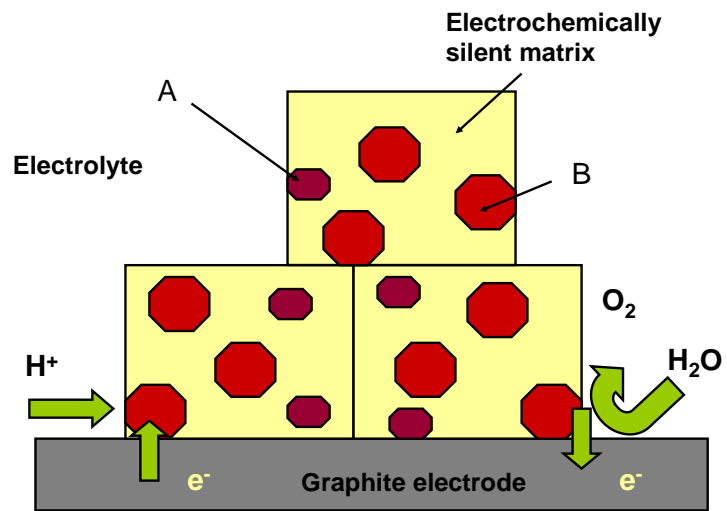
Figure 8.

Figure 9.

Click here to access/download

Supporting Information

ElettroanalysisRed Slip[SupplInform].doc